Absolute Molecular Orientational Distribution of the Polystyrene Surface

Kimberly A. Briggman, John C. Stephenson, William E. Wallace, and Lee J. Richter*

National Institute of Standards and Technology, 100 Bureau Drive, Gaithersburg, Maryland 20899-8372

Received: October 12, 2000; In Final Form: December 29, 2000

Vibrationally resonant sum frequency generation (VR-SFG) has been used to study the absolute molecular orientational distribution of the pendant phenyl groups at the free surface of polystyrene (PS) thin films on oxidized Si substrates. Characterization of the dependence of the VR-SFG on film thickness allows unique identification of the origin of the signal, e.g., free surface, bulk, or buried interface. For films <400 nm thick, the dominant source of vibrationally resonant signal is the PS/air interface, while the dominant source of the nonresonant background is the Si/SiO_2 interface. VR-SFG of a self-assembled phenylsiloxane layer is used to calibrate the relative phase between the vibrationally resonant phenyl ring hyperpolarizability and the Si/SiO_2 interface nonresonant hyperpolarizability. It is found that the phenyl groups are ordered at the PS/air interface and are oriented away from the polymer film. Quantitative analyses of the orientational distribution for both the PS free interface and the phenylsiloxane monolayer are reported. The phenyl groups at the PS free surface are tilted away from the surface normal in an angular range near 57°.

I. Introduction

It is widely acknowledged that the properties and behavior of surfaces and interfaces are critical to the processing characteristics and service performance of most polymer systems.[1,2] However, molecular characterization of these critical interfaces has proven difficult, presenting a barrier to complete scientific understanding and proper engineering design in many applications. Conventional molecular probes using X-rays, neutrons, or linear vibrational spectroscopies do not have the specificity to routinely characterize the interface in the presence of the bulk polymer. Charged particle probes, such as electron spectroscopies and secondary ion mass spectrometry, have adequate specificity but require a restrictive sample environment. Consequently, our present understanding of the molecular structure of polymer surfaces is based extensively on surfaces prepared in a vacuum. Near-edge X-ray absorption fine structure[3] (NEXAFS) is currently the leading electron spectroscopy applied to polymers. However, while NEXAFS can be used to determine bond alignment (angle of tilt) with respect to the free surface normal, it cannot return the orientation, or sense of the bond direction. This, in turn, leads to ambiguities in data interpretation.

Vibrationally resonant sum frequency generation (VR-SFG) has emerged as a powerful tool for the study of the molecular structure of interfaces.[4] As a second-order nonlinear optical technique, VR-SFG has inherent interface specificity: signals from centrosymmetric bulk regions are symmetry forbidden in the dipole approximation. Additionally, VR-SFG has the advantage, with respect to linear optical techniques, that it can determine both the orientation of functional groups at a surface and their alignment. Recently, VR-SFG has been applied to the study of the free surface of polymer substrates, establishing the alignment of surface chains,[5,6] the chemical composition of the surface,[7] and processing induced molecular changes in the surface.[8] In general, the surfaces of polymers are found to have sufficient polar order to produce readily detectable VR-SFG signals. Previous VR-SFG measurements have been performed on either bulk substrates or thin films on fused silica substrates. Surprisingly, these studies have not measured the absolute orientation of the functional groups at the surface although chemical arguments have been presented[5,6] to advocate particular molecular orientations. The weak nonresonant background in these systems makes absolute orientation measurements difficult.

In this paper we report VR-SFG measurements of polystyrene (PS, $[CH_2CH(C_6H_5)]_n$) thin films on oxidized silicon substrates. Characterization of the dependence of the VR-SFG response on film thickness allows unique identification of the origin of the signal. For films <400 nm thick, the dominant source of vibrationally resonant signal is the PS/air interface; while the dominant source of the nonresonant background is the Si/SiO_2 interface. The nonresonant sum frequency mixing at the Si/SiO_2 interface provides a convenient phase reference for the characterization of the PS surface. Calibration of the phase reference with a phenylsiloxane self-assembled layer allows the determination of the absolute orientation of the pendant phenyl groups at the PS surface.

II. Experiment

The experiments were performed with a broad-bandwidth SFG apparatus that has been described earlier.[9] In brief, broad-bandwidth (>150 cm^{-1} FWHM) 3 μm IR pulses, derived from a ~100 fs, 1 kHz, regeneratively amplified Ti-sapphire laser system, are temporally and spatially overlapped with narrow-bandwidth (~3 cm^{-1}) 792 nm (VIS) pulses at the sample. The reflected sum-frequency light is collected, dispersed in a 0.75 m spectrograph, and detected with a scientific grade CCD array detector. This allows the simultaneous acquisition of a >300 cm^{-1} wide SFG spectrum. In this work, the IR and VIS pulse energy, beam diameter, and angle of incidence were typically: 4 μJ, 100 μm, 54°, and 1 μJ, 150 μm, 36°, respectively. The IR and Raman spectra were acquired with a Nicolet Magna-IR 860 FTIR at 2 cm^{-1} resolution and a Bruker RFS100 FT-Raman (1064 nm excitation) at 2 cm^{-1} resolution, respectively.[10]

* Corresponding author: lee.richter@nist.gov.

10.1021/jp0037495
Published on Web 03/17/2001

The polymer samples were 220 500 g mol^{-1} number-average molecular mass, narrow-distribution atactic PS, spin coated at 2000 rpm from toluene solutions onto oxidized Si(100) wafers and annealed under vacuum for 2 h at 120 °C. The Si substrates were prepared by either UV−ozone oxidation of HF stripped wafers (producing a nominally 2 nm thick SiO_2 film), or by chemical-mechanical polishing of a thick chemical vapor deposited (CVD) SiO_2 film (producing a 340 nm film). All PS and SiO_2 film thicknesses were determined by spectroscopic ellipsometry and are accurate to 1−2 nm. To remove recurring surface contamination, the free surfaces were rinsed with ethanol and N_2 dried prior to each measurement. The phenylsiloxane monolayers were prepared by silanization of the 340 nm SiO_2 surface. Triethoxyphenylsilane (0.5 mL) was dissolved in a mixture of acetone (50 mL) and water (5 mL) to which 125 μL of hydrochloric acid had been added to aid hydrolysis. This mixture was allowed to stir for 1 h. The silicon oxide surfaces were cleaned by rinsing in acetone and in methanol, exposed in a UV−ozone cleaner for 6 min, placed in an equal volume mixture of concentrated hydrochloric acid and methanol for 10 min and in concentrated sulfuric acid for 10 min, and finally boiled in deionized water for 10 min. The cleaned samples were then placed in the silane mixture for 20 min, subsequently rinsed in acetone and heated in air at 90 °C for 20 min. Sessile water drop contact angles on these monolayers were 66° ± 2° (unless otherwise noted, all uncertainties are reported as 1 σ), suggestive of a phenyl-terminated surface and consistent with other aromatic organosilane monolayers.[11]

III. Theory

In classical, macroscopic theory the electric field created at the sum frequency arises from an induced polarization P in a material. For an optical quality thin film, there are four possible locations of this induced polarization: at the air/film interface, in the bulk of the film, at the film/substrate interface, and in the bulk of the substrate. In general, the polarization at each location is given by

$$P_i(\omega_{SUM} = \omega_{VIS} + \omega_{IR}, r) = \chi^{D}_{ijk} E_j(\omega_{VIS}, r)\, E_k(\omega_{IR}, r) + \chi^{Q1}_{ijkl} E_j(\omega_{VIS}, r) \nabla_k E_l(\omega_{IR}, r) + \chi^{Q2}_{ijkl} E_j(\omega_{IR}, r) \nabla_k E_l(\omega_{VIS}, r) + \nabla_j \chi^{Q}_{ijkl} E_k(\omega_{VIS}, r)\, E_l(\omega_{IR}, r) + \ldots \quad (1)$$

where χ^{D} is the local dipole response and is expected to dominate the interface polarization when symmetry allowed. In locally centrosymmetric (bulk) films (amorphous PS, amorphous SiO_2, and Si) χ^{D} is symmetry forbidden, and the leading order contributions come from the quadrupolar terms χ^{Q}.[12] The dipolar contributions from the interfaces and the quadrupolar contributions from the bulk can be of comparable magnitude. It is therefore critical to determine the origin of the induced polarization. A number of approaches to this problem have been developed.[12] The most commonly adopted is to modify the surface in some fashion (typically via exposure to solvent) and if the signal changes, it is attributed to the free interface. A more comprehensive approach to this problem is to characterize the signal as a function of film thickness.[13]

The electric field at the sum frequency, arising from an infinitely thin nonlinear sheet, can be shown to be

$$E_l(\nu_{SUM}) = \frac{i8\pi^3}{\lambda^2 k_z(\nu_{SUM})} \chi^{D}_{ijk}(\nu_{SUM} = \nu_{VIS} + \nu_{IR}) F^{\diamond}_{il}(\nu_{SUM}) \times F_{jm}(\nu_{VIS})\, F_{kn}(\nu_{IR})\, E_m(\nu_{VIS})\, E_n(\nu_{IR}) \quad (2)$$

where $k_z(\nu_{SUM})$ is the component of the wavevector of the sum-frequency plane wave along the surface normal, F_{jm} and F_{kn} are the conventional Fresnel transfer matrix relating the incident fields $E_{m,n}(\nu)$ to the fields at the nonlinear sheet, and $F^{\diamond}_{il}$ is a transfer matrix for the emission of the sum-frequency. $F^{\diamond}_{il}$ can be calculated by many routes; in this work, we use the Green's function approach of Sipe.[14] We have adopted the convention that the local field corrections are folded into the definition of χ. Shown in Figure 1 are calculations of the total Fresnel factor weight (e_l is a unit vector along l):

$$|F| = \left| \frac{i8\pi^3}{\lambda^2 k_z(\nu_{SUM})} F^{\diamond}_{il} F_{jm} F_{kn} e_l e_m e_n \right|$$

for lmn = SSP and SPS polarization configurations for a nonlinear polarization sheet located just within the PS layer either at the free or the buried interface or uniformly distributed through the bulk as a function of PS film thickness t. The strong oscillations are a result of thin film interferences in both the driving electric fields and the emitted sum-frequency (SF) field. The interference pattern in the Fresnel factors appears simple over this limited range in film thickness. The interference in the sum frequency and the visible input are not resolved (they contribute to the breadth of the features) and the interference in the IR input is not important since the IR field is roughly constant over the range of thickness used in our experiments, unlike the other two fields. The pronounced maxima for the SSP configuration from the free surface (shown in Figure 1a) for $t \sim 120$ and 350 nm arise primarily from the constructive interference between the directly emitted SF and the SF reflected from the Si/SiO_2/PS interface. Near 350 nm, extrema occur for all three polarization combinations: SSP, SPS, and PSS, suggesting that this is an optimal film thickness for experimental study. Under the assumption that the interface and bulk structures are independent of film thickness (met for polymer films thicker than ≈6 times the radius of gyration[15]), these calculations indicate that the origin of the SF generation can be readily determined by characterizing the variation of the signal with t. The radius of gyration for the PS used in this study is 13 nm.[16]

For an azimuthally symmetric sample, there are only 4 elements in the nonlinear susceptibility χ^{D}_{ijk}: zzz, $xxz = yyz$, $xzx = yzy$, $zxx = zyy$. The three polarization combinations: SSP, SPS, and PSS are each uniquely determined by the single χ^{D} elements: xxz, xzx, and zxx, respectively. For each of these three polarization combinations, the spectrum can be modeled by

$$\text{signal} = \left| B_{nr} e^{i\varphi} + \sum_r \frac{A_r}{\nu - \nu_r + i\Gamma_r} \right|^2 \sim |F_{nr}\chi^{D}_{nr} + F_r \chi^{D}_r|^2 \quad (3)$$

where F_{nr}, χ^{D}_{nr}, F_r, and χ^{D}_r are the nonresonant and resonant Fresnel factors and nonlinear susceptibilities. B_{nr} arises from nonresonant contributions to χ^{D}_{nr}, and A_r, ν_r, and Γ_r are the amplitude, center wavenumber, and line width (HWHM), respectively, for resonant vibrational mode r. Within the usual approximation that there are no relevant visible resonances in the hyperpolarizabilty, A_r and B_{nr} are real numbers. The terms A_r, B_{nr}, and φ reflect both the relevant χ^{D} and the Fresnel factor weights. To within experimental error, our spectra indicate that Kleinmann symmetry[17] holds for the SUM and VIS indices of χ^{D}, i.e., $\chi^{D}_{xzx} \sim \chi^{D}_{zxx}$.

In a polar ordered molecular system, the macroscopic resonant χ^{D}_r can be modeled as the orientational average of a molecular

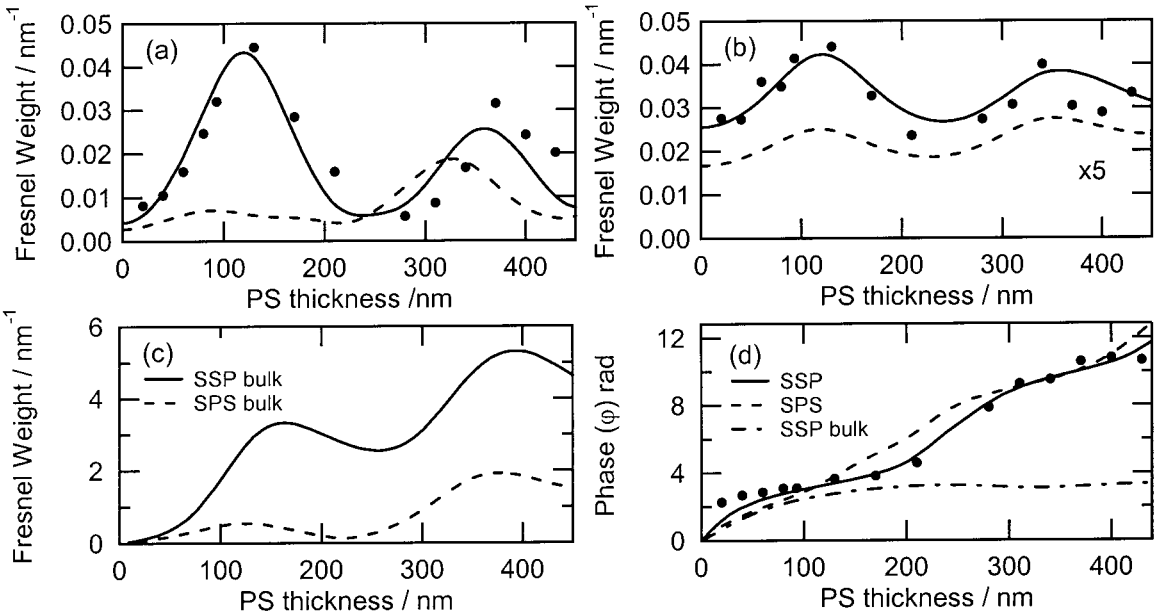

Figure 1. Absolute value of the Fresnel factor weights: $|F^{\diamond}_{il}F_{jm}F_{kn}e_le_me_n|$ for the SFG signal arising from (a) the free interface, (b) the SiO_2/Si interface, and (c) the bulk of a PS film on a 2 nm SiO_2 terminated Si substrate, as a function of PS film thickness. Shown in (d) is the relative phase between Fresnel factor weights for the free interface and the SiO_2/Si interface (solid line is SSP; dashed line is SPS). The solid points in (a) are the SSP polarized SFG amplitudes A_r for ν_2 of PS and in (b) are the nonresonant amplitudes B_{nr} as described in the text, scaled to agree with the peak of the respective curves. The solid points in (d) are the experimental relative phase values as described in the text.

hyperpolarizability β: $\chi^{D}_{ijk} = N\langle\beta_{lmn}R_{li}R_{mj}R_{nk}\rangle$ where R is a rotation matrix relating the internal coordinates of the molecule to the lab coordinates and N is the number density. When neither the SUM nor VIS frequencies are near resonances in the molecule, β can be approximated by

$$\beta_{ijk} = \frac{1}{2}\frac{\alpha_{ij}\,\mu_k}{(\nu - \nu_r + i\Gamma_r)} \tag{4}$$

where α is the dynamic Raman polarizability, and μ the infrared transition dipole moment of vibrational mode r.[18]

IV. Results

Shown in the lower panel of Figure 2 are the SFG spectra in the SSP and SPS polarization combinations of a 370 nm PS film on a nominally 2 nm silicon oxide terminated Si wafer. The raw spectra have been normalized to the SSP polarized SFG spectrum of a Au film covered with a 120 nm fully deuterated PS film to correct for the spectral envelope of the IR pulse. Similar spectra have been reported by Zhang, et al. for PS films on silica.[19] The primary features are attributed to the fundamental aromatic CH stretching modes of the pendant phenyl groups. The observation of the SFG signal clearly establishes that there is polar ordering of the phenyl groups at the surface, and therefore, the phenyl groups are not rotationally symmetric about the chain backbone that must lie in the surface plane. Also shown in Figure 2 are fits of the spectra to eq 3, including seven resonant components and a linearly varying nonresonant background. The imaginary parts of the resonant components are displayed to indicate the amplitude, width, and sign of each component. The SPS and SSP spectra were fit simultaneously to a common set of ν_r and Γ_r. Table 1 summarizes the results from analyzing the SFG spectra in Figure 2. The reported uncertainties in the fit parameters are one standard deviation, derived from the elements of the inverse of the curvature matrix.[20] All frequencies are consistent with lines present in the Raman and IR spectra of bulk PS shown in the

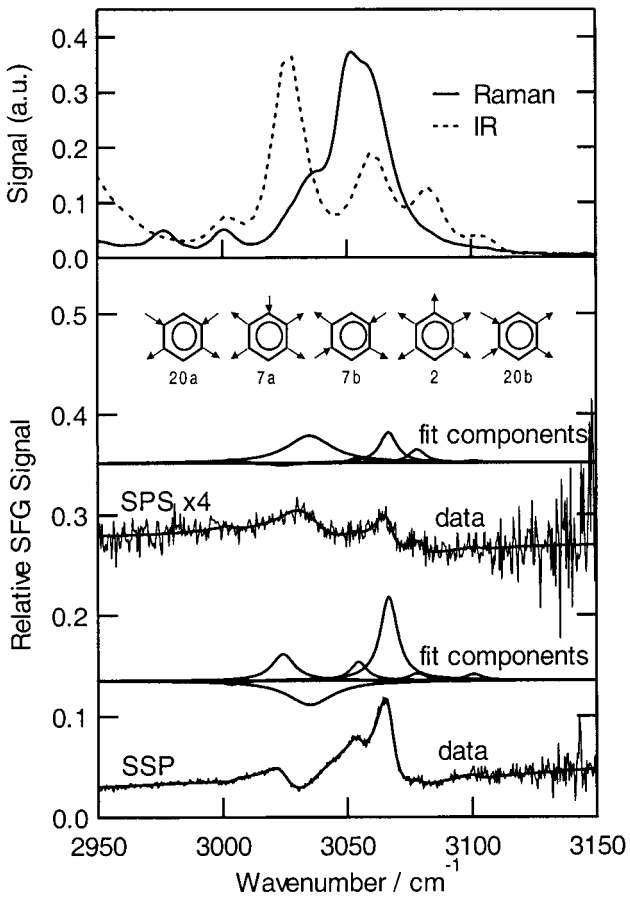

Figure 2. Upper: Raman spectrum and IR spectrum of bulk PS. Lower: SSP and SPS polarized SFG spectra of a 370 nm PS film on a 2 nm SiO_2 layer on Si. The SPS spectrum has been offset for clarity and scaled by a factor of 4. The solid lines are fits as described in the text. Also shown are the imaginary parts of the individual components of the fits (arbitrarily scaled). Inset: schematic of the phenyl ring CH stretching normal modes.

TABLE 1: Line Fit Results and Assignments for Polystyrene SFG Spectra

				bulk PS ν (cm^{-1})			
ν (cm^{-1})	Γ (cm^{-1})	A_{ssp}	A_{sps}	IR	Raman	DFT ν (cm^{-1})	assignment/symmetry
3004.2 ± 0.8	4 ± 1	−0.03 ± 0.01	−0.01 ± 0.01	3000	3000		cb[a]
3024.2 ± 0.3	5.5 ± 0.5	0.29 ± 0.05	−0.01 ± 0.01	3027		3155.4	ν_{20a}/A1
3035.0 ± 0.8	11 ± 1	−0.52 ± 0.09	0.30 ± 0.04		3034	3169.8	ν_{7a}/A1
3054.5 ± 0.2	4.2 ± 0.3	0.15 ± 0.03	0.01 ± 0.01		3050	3157.3	ν_{7b}/B1
3066.7 ± 0.2	4.1 ± 0.1	0.69 ± 0.02	0.12 ± 0.01	3060	3060	3190.9	ν_2/A1
3078.2 ± 0.8	4 ± 1	0.06 ± 0.04	0.05 ± 0.03	3083		3178.1	ν_{20b}/B1
3101 ± 2	4 ± 2	0.05 ± 0.07	0.01 ± 0.03	3104			cb[a]
ϕ		10.03 ± 0.08	10.04 ± 0.2				
B @ 3065 cm^{-1}		0.202 ± 0.001	0.162 ± 0.001				

[a] Combination band.

upper panel of Figure 2. Table 1 also summarizes our assignment of the features. Wilson's notation for the normal modes of benzene is used;[21] the inset in Figure 2 schematically indicates the CH displacements in the normal modes. There is considerable disagreement in the literature on the assignment of the aromatic CH stretches of PS.[22] Our assignment is based on ab initio Hartree−Fock (HF) and density functional theory (DFT) calculations for toluene,[23] and the polarization dependence of the SFG spectra (see below). The level of calculation employed accurately predicts the observed *harmonic* frequencies[24] and IR and Raman intensities for benzene.[25] The *unscaled* frequencies from the DFT calculations are also presented in Table 1. The anharmonic correction for the fundamentals has been estimated to be 117 cm^{-1} in benzene[25] and is expected to be similar for the monosubstituted phenyl side group. The assignment of ν_2 is straightforward, as it is the only mode with both significant calculated Raman and IR intensity. The assignments of ν_{7a} and ν_{7b} are based on their strong calculated Raman intensity, and the polarization behavior of the SFG spectra. The assignment of ν_{20a} and ν_{20b} is based on their calculated IR intensities and frequency ordering; however, this ordering is inconsistent with Varsanyi.[26] Our calculations invert the order of the pairs: (ν_{7a}, ν_{7b}) and (ν_2, ν_{20b}). Our calculation, in the double harmonic approximation, neglects anharmonicity and Fermi resonances. The IR spectrum of benzene is severely affected by multiple Fermi resonances;[27] they may be the origin of poor correlation between theoretical and experimental frequencies for the monosubstituted phenyl side group.

Shown in Figure 1a is the comparison of the amplitudes A_r of the ν_2 mode from fitting SSP polarized SFG spectra of a series of variable thickness PS films on the 2 nm silicon oxide substrate with the calculated Fresnel factor weights $|F|$ as a function of PS film thickness. The data have been normalized to the calculated model at the peak. The overall good agreement between the experimental A_r and $|F|$ calculated for the free surface clearly establishes that over the film thickness range studied, the signal is always dominated by contributions from the free surface. Similar analyses of the other resonant features in the SFG spectra indicate the signal originates at the free surface. Note from Figure 1b that the sensitivity to the buried interface in a single layer system is significantly less than the free surface. Shown in Figure 1b are the experimental nonresonant background amplitudes, B_{nr}, from the same series, evaluated at 3065 cm^{-1}. Again, a single normalization factor has been applied. The good agreement between B_{nr} and $|F|$ calculated for the silicon oxide interface shows that the nonresonant background arises from the buried interface/substrate and is attributed to contributions from the silicon oxide interface and quadrupolar mixing in the Si itself. When the resonant and nonresonant contributions to the spectrum are from spatially distinct regions, the relative phase φ between them (eq 3) becomes a function of the sample structure. Shown in Figure 1d is the calculated relative phase between the nonlinear Fresnel factors for the free and buried interfaces in the SSP polarization combination. Also shown are the experimentally determined phases between the nonresonant background and the resonant features. The phase difference between the χ_r and χ_{nr}, $\Phi \equiv \mathrm{Arg}(\chi_{nr}/\chi_r)$, is the vertical offset between the experimental points and the line in Figure 1d and is ∼0.2 rad ±0.2 rad.

The phase difference between the resonant and nonresonant SFG signals can be used to determine the vector orientation of the phenyl groups at the surface.[28] However, this requires knowledge of the phase difference between the second-order susceptibility of the SiO_2/Si interface and the hyperpolarizability of the pendant phenyl group. We have chosen to calibrate the phase difference with a reference system, consisting of a self-assembled monolayer (SAM) of phenylsiloxane silanized onto an oxidized Si substrate. In the SAM, the phenyl ring is bound to the SiO_2 via a Si group and should be directed away from the substrate due to the silane coupling chemistry. Outward oriented phenyl groups are consistent with the observed water contact angles. Shown in the lower panel of Figure 3 are the SSP and SPS polarized SFG spectra of a phenylsiloxane SAM formed on a 340 nm CVD SiO_2 layer on a Si substrate. Also shown are the fits to eq 3, using three resonant components. The results of the fits are summarized in Table 2. Shown in the upper panel of Figure 3 are reference Raman and IR spectra of the triethoxyphenylsilane (neat liquid) used to form the SAM. The assignment of the SFG, IR, and Raman spectra is based on HF and DFT calculations for monophenylsilane, and the assignments by Durig, et al. for monophenylsilane.[29] The assignment of ν_2 is again straightforward, given its strong calculated Raman and IR intensities. The assignment of the remaining lines is based primarily on the correlation with calculated IR intensities, and the symmetry assignments of Durig, et al. With the exception of the reversal of ν_2 and ν_{20b}, the calculations and experiments are in good agreement with respect to the frequency ordering. Our assignment differs from Durig et al. by the exchange of 7b with 20b. Only the symmetry of the feature at 3038 cm^{-1} is essential to the analysis that follows.

The optical thickness and index of refraction of the 340 nm CVD SiO_2 layer in Figure 3 is comparable to that of the PS layer in Figure 2, and thus the shape of the spectra, determined by the relative phase φ, can be directly compared. The similarities in Figures 2 and 3 clearly indicate that φ is similar in the two cases and therefore establish that the phenyl groups at the PS surface point in the same direction as those in the SAM; i.e., they are directed away from the substrate. We will define the direction of the phenyl ring by the direction of the C to H bond vector of the para H. This is the z′ direction in the coordinate system defined in the inset of Figure 3. The phase

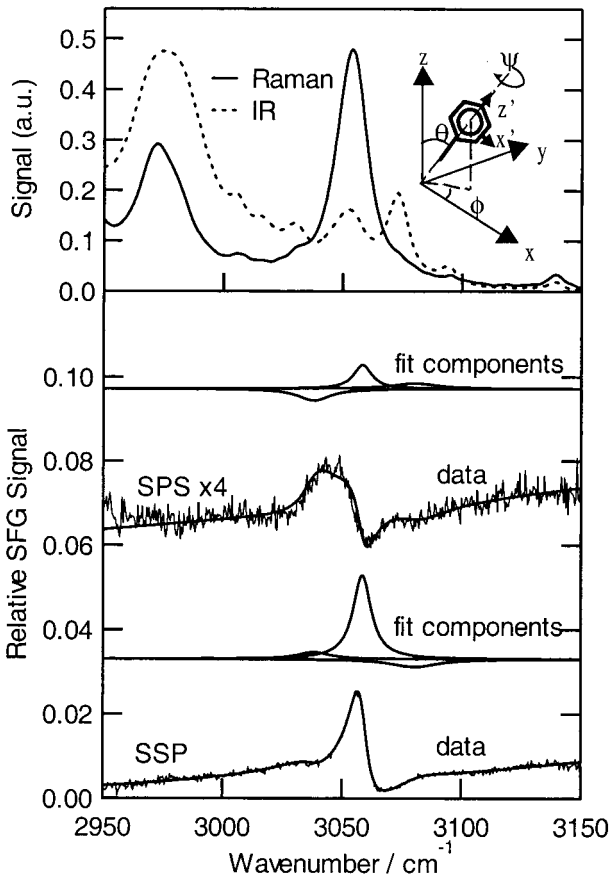

Figure 3. Upper: Raman spectrum and IR spectrum of triethoxyphenylsilane. Lower: SSP and SPS polarized SFG spectra of a phenylsiloxane SAM on a 340 nm SiO_2 layer on Si. The SPS spectrum has been offset for clarity and scaled by a factor of 4. The solid line is a fit as described in the text. Also shown are the imaginary parts of the individual components of the fit (arbitrarily scaled). Inset: definition of the right-handed coordinate systems used in the text.

differences between χ_r^D and χ_{nr}^D (derived from the experimental φ) for the respective PS and SiO_2 optical thickness in Figures 2 and 3 are $\Phi_{xxz}^{PS} = 0.0$ rad $\pm$ 0.1 rad, $\Phi_{xxz}^{SAM} = -0.5$ rad $\pm$ 0.2 rad, $\Phi_{xzx}^{PS} = 0.0$ rad $\pm$ 0.2 rad, and $\Phi_{xzx}^{SAM} = -0.7$ rad $\pm$ 0.1 rad. The small systematic difference between the PS and SAM phases may be due to slight differences in the properties of the two silicon oxide interfaces. It may also be due to errors in calculating the Fresnel weight for the silane samples. The CVD SiO_2 layer thickness was visibly graded across the sample due to polishing. Ellipsometry indicated as much as a 10 nm variation in SiO_2 thickness across the samples. The absolute orientation of the PS is also supported by comparisons between PS films on Au substrates, and SAMs prepared from thiophenol on Au.

Insight into the alignment of the phenyl groups at the PS surface can be obtained by quantitatively analyzing the ratios of the lines observed in SPS and SSP polarizations to determine the susceptibility ratio $\chi_{xzx}^D/\chi_{xxz}^D$. The susceptibility ratio can be calculated for trial orientational distributions given the molecular β (see below). Assuming local C_{2v} symmetry for the phenyl ring significantly simplifies α and μ and thus β. Three terms contribute to β_{ijk} for the A_1 symmetry species, $\beta_{ijk} = \beta_{z'z'z'}, \beta_{x'x'z'}$, and $\beta_{y'y'z'}$, and only one contributes to the B_1, $\beta_{x'z'x'} = \beta_{z'x'x'}$. As the out-of-plane Raman polarizability is very weak,[30] the $\beta_{y'y'z'}$ term for the A_1 modes will be subsequently neglected. Proper averaging of the β's results in χ^D tensors that obey permutation symmetry of the SUM and VIS indices, i.e., $\chi_{zxx}^D = \chi_{xzx}^D$; therefore there are only three independent observables for the A_1 modes. For the B_1 modes an additional constraint appears, $\chi_{zzz}^D = -1/2\chi_{xxz}^D$, reducing the number of independent observables to two for these modes. Shown below are the transformations between β and χ^D as a function of the tilt of the z' axis of the phenyl ring θ and its twist ψ out of the plane of tilt. The azimuthal angle ϕ has been averaged out, based on the assumption of an isotropic surface (the inset to Figure 3 defines the angles θ, ψ, and ϕ; the coordinates in the molecular frame are primed).

$$A_1: \quad \chi_{zzz} = N(\beta_{x'x'z'}\langle\cos\theta \sin^2\theta \cos^2\psi\rangle + \beta_{z'z'z'}\langle\cos^3\theta\rangle)$$

$$A_1: \quad \chi_{xxz} = \frac{N}{8}(\beta_{x'x'z'}\langle\cos\theta(3 + \cos 2\theta - 2\sin^2\theta\cos 2\psi)\rangle + 4\beta_{z'z'z'}\langle\cos\theta\sin^2\theta\rangle)$$

$$A_1: \quad \chi_{xzx} = -\frac{N}{2}(\beta_{x'x'z'}\langle\cos\theta \sin^2\theta \cos^2\psi\rangle - \beta_{z'z'z'}\langle\cos\theta\sin^2\theta\rangle)$$

$$B_1: \quad \chi_{xxz} = -N\beta_{x'z'x'}\langle\cos\theta \sin^2\theta \cos^2\psi\rangle$$

$$B_1: \quad \chi_{xzx} = \frac{N}{2}\beta_{x'z'x'}\langle\cos^3\theta - \cos\theta\sin^2\theta\cos 2\psi\rangle \qquad (5)$$

The Fresnel weights necessary to obtain $\chi_{xzx}^D/\chi_{xxz}^D$ from A_{sps}/A_{ssp} are presented in Table 3 for the samples in Figures 2 and 3. Summarized in Table 4 are the susceptibility ratios for the two systems, PS and phenylsiloxane. The uncertainties are one standard deviation for two independently prepared samples and are dominated by sample-to-sample variation in the spectra; hence, some entries in Table 4 differ from those deduced only from Tables 1 and 2. For the PS surface, the features assigned to ν_{7a} and ν_2 at 3034 and 3067 cm^{-1} are the most statistically robust. Both modes are of A_1 symmetry; assuming a narrow orientational distribution, the ratio of $\chi_{xzx}^D/\chi_{xxz}^D$ is determined by three parameters: θ, ψ, and the ratio $\rho = \beta_{z'z'z'}/\beta_{x'x'z'}$. The hyperpolarizability ratios ρ calculated for both modes, based on eq 4 and α and μ from the HF and DFT calculations on toluene, are $\rho_{\nu2}^{HF} = 1.07$, $\rho_{\nu2}^{DFT} = 1.13$, $\rho_{\nu7a}^{HF} = -0.26$, and $\rho_{\nu7a}^{DFT} = -0.25$. The value for $\rho_{\nu2}$ is consistent with previous estimates for benzoate ions based on bond additive polarizabilities.[31] Using the theoretical values of ρ, the extracted $\chi_{xzx}^D/\chi_{xxz}^D$ for the two modes constrain θ and ψ to lie in the ranges 49−65° and 45−51°, respectively. The range is reflective of the uncertainty in the $\chi_{xzx}^D/\chi_{xxz}^D$ ratio, and the range of calculated ρ's. It should be noted that the ratio $\chi_{xzx}^D/\chi_{xxz}^D$ for a narrow distribution about $\psi = 45°$ is indistinguishable from an isotropic distribution in ψ. If one independently analyzes the $\chi_{xzx}^D/\chi_{xxz}^D$ ratios, assuming an isotropic distribution in ψ, one obtains tilt angles from ν_2 of 48−90° and from ν_{7a} of 47−56° (again, the range reflects the variation in both experimental amplitudes and calculated ratios). When the tilt angle is estimated from macroscopic optical measurements, surface roughness can contribute to the effective width of the orientational distribution.[32] For second harmonic generation[33] and SFG, rough surfaces (and broad distributions) produce apparent tilt angles of ~39° independent of mean tilt when narrow distributions are assumed. The high tilt angles observed indicate that roughness is not important, consistent with the measured rms roughness of the PS films: 0.5−0.8 nm.

A similar analysis can be applied to the phenylsiloxane layer. The features assigned to ν_{7b} and ν_2 at 3038 and 3058 cm^{-1} are

TABLE 2: Line Fit Results and Assignments for Phenylsiloxane SFG Spectra

				liquid ν (cm^{-1})			
ν (cm^{-1})	Γ (cm^{-1})	A_{ssp}	A_{sps}	IR	Raman	DFT ν (cm^{-1})	assignment/symmetry
				3005	3005		cb[a]
				3015		3155.9	ν_{20a}/A1
3038.2 ± 0.3	8.1 ± 0.8	0.13 ± 0.02	−0.11 ± 0.01	3030	3030	3157.6	ν_{7b}/B1
3058.5 ± 0.1	4.6 ± 0.1	0.91 ± 0.01	0.13 ± 0.01	3052	3054	3191.6	ν_2/A1
3080 ± 1	11 ± 2	−0.21 ± 0.04	0.07 ± 0.01	3074		3170.2	ν_{7a}/A1
				3094	3096	3180.2	ν_{20b}/B1
				3138	3139		cb[a]
ϕ		8.63 ± 0.04	8.46 ± 0.08				
B @ 3065 cm^{-1}		0.078 ± .001	0.070 ± .001				

[a] Combination band.

TABLE 3: Fresnel Weights Used in Analysis of Figure 2 and Figure 3

layer 1	layer 2	F_{ssp} (nm^{-1})	F_{sps} (nm^{-1})
370 nm, $n = 1.568$	1.5 nm, $n = 1.45$	−0.0100 + 0.0226 I	−0.0034 + 0.0126 I
1 nm, $n = 1.568$	340 nm, $n = 1.45$	0.0092+ 0.0162 I	0.0138+ 0.0174 I

TABLE 4: Susceptibility Ratios

polystyrene		phenylsiloxane	
ν (cm^{-1})	$\chi^D_{xzx}/\chi^D_{xxz}$	ν (cm^{-1})	$\chi^D_{xzx}/\chi^D_{xxz}$
3025 ± 1	−0.35 ± 0.33		
3033 ± 4	−0.9 ± 0.2	3037.9 ± 0.3	−0.7 ± 0.2
3055 ± 1	−0.5±.9	3058.9 ± 0.6	0.12 ± 0.01
3067.0 ± 0.6	0.31 ± 0.05	3080 ± 1	−0.2±.2
3080 ± 4	1.2 ± 0.5		

the most statistically robust. (See Table 4.) The ratio of $\chi^D_{xzx}/\chi^D_{xxz}$ for B_1 modes is determined solely by θ and ψ (assuming a narrow orientational distribution). Simultaneously fitting the observed $\chi^D_{xzx}/\chi^D_{xxz}$ for ν_{7b} and ν_2 (taking $\rho_{\nu 2}$ from the theoretical calculations of phenyl silane: $\rho^{HF}_{\nu 2} = 1.08$, $\rho^{DFT}_{\nu 2} = 1.16$) defines θ and ψ to lie in the ranges 37−39° and 26−31°, respectively. Again, this reported range is reflective of the uncertainty in the $\chi^D_{xzx}/\chi^D_{xxz}$ ratio and the range of calculated ρ's. Unlike the PS data, the phenylsilane spectra are not consistent with an isotropic distribution in ψ. The rms roughness of the samples, after deposition of the phenylsilane monolayer was 1.5 nm, slightly greater than that of the PS surfaces.

V. Discussion

Atomistic computer simulations have been made of atactic polypropylene surfaces.[34] At the microscopic level, the interface is remarkably abrupt. The density profile varied in a sigmoidal fashion from bulk to zero over only a 1 nm region. Within that region, it was found that there was a slight preference for the C−C bonds in the backbone to lie in the plane of the surface, presumably to maximize the cohesive interaction between the surface layers and the bulk. The order parameter $S \equiv {}^1/_2(3\langle\cos^2\theta\rangle - 1)$ for the C−C bonds was ≈−0.1. The pendant methyl groups in polypropylene were found to have a slight preference for alignment perpendicular to the surface plane, $S \approx 0.15$. Unfortunately, the order parameter does not provide insight into the vector orientation of the pendant methyl groups. The simulations indicated that the distribution of rotational states of the skeletal bonds was perturbed in the interface region; the number of trans states decreased and the number of gauche states increased, to allow "reflection" of the chain by the vacuum, into the more energetically preferred bulk.

We have not attempted to calibrate the absolute magnitude of the SFG signals observed for the different SiO_2 samples. However, the amplitude of the resonant signal of ν_2 for the PS surface is nominally the same as that of the phenylsiloxane SAM, suggesting that the number of phenyl groups in the ordered distribution is of the order of a monolayer. This is consistent with the thin interface region in the atomistic simulations. The observation that the phenyl ring is oriented away from the substrate, coupled with the expected decrease in density across the surface region, suggests that the pendant group "seeks out" the higher free volume region. It is unclear if this is due to entropic considerations or actually arises due to cohesive interactions between the chain backbone and the film. Orientation of the phenyl ring away from the substrate may also be the most energetically favorable way to reduce the abrupt change in mass density induced by the free surface. It is notable that the Lorentzian width (HWHM) of the ν_2 SFG feature (Γ = 4.4 cm^{-1}) is narrower than the Lorentzian widths of the bulk IR and Raman spectra (Γ = 6−8 cm^{-1}), implying less inhomogeneous broadening of ν_2 for the surface phenyl groups. Additionally, there is a systematic ~7 cm^{-1} blue shift of ν_2 at the free surface compared to the bulk of the film. This may reflect the lower density environment of the pendant groups at the surface.

Both angle-resolved ultraviolet photoelectron spectroscopy (ARUPS)[35] and NEXAFS[36,37] have been applied to study of the alignment of the π system of the phenyl pendant group at PS free surfaces. In both cases, the films were thin in order to avoid charging, and hence not directly comparable to our samples. These electronic spectroscopies can only determine the alignment of the plane of the ring. In the ARUPS study of 10 and 27 nm PS films, the alignment varied with film thickness. The 10 nm film was consistent with a completely isotropic distribution of the ring plane, while the 27 nm film indicated the alignment distribution was very broad, but peaked with the plane of the ring perpendicular to the surface. The ARUPS study suggested that the average angle β' between the surface normal (z axis in Figure 3) and an axis normal to the plane of the phenyl ring (y' axis in Figure 3) was ≈55° for the 27 nm film.[35] Using the Euler transformation $\cos(\beta') = \sin(\theta)\sin(\psi)$, our values of $\theta \approx 57°$, and $\psi \approx 48°$ imply a value of $\beta' \approx 51°$, in good agreement. In the NEXAFS study of <100 nm PS films, a distribution favoring the ring plane perpendicular to the surface was also suggested.[36] In a study of unannealed, spin-cast films[37] a tilt of the ring plane from the surface normal of 30° ($\beta' \approx 60°$) was observed in the surface region. The ring plane was even closer to the surface normal ($\beta' \approx 63°$) in the bulk of the unannealed films. Neither ARUPS nor NEXAFS experiments determined θ, and the linear, dipolar techniques cannot determine the sign of θ. A combined NEXAFS and SFG study of

identical films could provide greater insight into the spatial distribution of the surface order as the linear and nonlinear techniques probe different moments of the orientational distributions.

VR-SFG has previously been applied to the study of free surfaces of polypropylene (PP)[6] and poly(vinyl alcohol),[5] both of which are simple pendant group polymers. Atactic PP would be expected to behave comparably to atactic PS, as both are glassy polymers, with relatively weakly interacting pendant groups. Analysis of the alignment of the pendant methyl group in PP indicated a tilt θ of 30°, while analysis of the methylene backbone indicated a tilt θ of 59° of the methylene group. On the basis of these results, it was proposed that the chain backbone lay in the plane of the surface, with the methyl directed away from the film, although an absolute phase measurement was not performed. The vibrational spectra of the side OH group in poly(vinyl alcohol) indicated hydrogen bonding; this suggested that the OH groups were directed into the film surface, with the complementary methylene groups on the nominally all trans chains directed outward. This was quantitatively supported by the determination of a tilt angle for the symmetric bisector of the methylene group near 0°.[38] The strong hydrogen bonding interaction makes poly(vinyl alcohol) very different from PP, and PS; it is a crystalline material.

VI. Conclusion

We present the first measured absolute molecular orientational distribution of a pendant side group at a polymer surface. At the PS−air interface, the pendant phenyl groups are oriented away from the film. This is in contrast to prior NEXAFS results that could not definitively determine whether the phenyl ring pointed toward or away from the substrate. The phenyl groups are suggested to point outward either as a means to seek the maximum free volume or possibly as the lowest free energy conformation that smooths out the abrupt change in density due to the presence of the free surface. The phenyl groups at the PS free surface were shown to be tilted away from the surface normal in an angular range near 57°.

Acknowledgment. We thank Dr. Steven J. Choquette for his assistance in the acquisition of the Raman spectra and Dr. Michael Fasolka for his assistance in the acquisition of AFM images. Kimberly Briggman is a NIST National Research Council postdoctoral research associate.

References and Notes

(1) Wool, R. P. *Polymer Interfaces: Structure and Strength*; Hanser: Munich, 1995.

(2) Jones, R. A. L.; Richards, R. W. *Polymers at Surfaces and Interfaces*; Cambridge University Press: Cambridge, U.K., 1999.

(3) Stöhr, J. *NEXAFS Spectroscopy*; Springer-Verlag: Berlin, 1992.

(4) Miranda, P. B.; Shen, Y. R. *J. Phys. Chem. B* **1999**, *103*, 3292. Richmond, G. L. *Anal. Chem.* **1997**, *69*, A536. Bain, C. D. *J. Chem. Soc., Faraday Trans.* **1995,** *91*, 1281.

(5) Wei, X.; Zhuang, X.; Hong, S.-C.; Goto, T.; Shen, Y. R. *Phys. Rev. Lett.* **1999**, *82*, 4256.

(6) Zhang, D.; Shen, Y. R.; Somorjai, G. *Chem. Phys. Lett.* **1997**, *281*, 394. Gracias, D. H.; Zhang, D.; Lianos, L.; Ibach, W.; Shen, Y. R.; Somorjai, G. A. *Chem. Phys.* **1999,** *245*, 277.

(7) Chen, Z.; Ward, R.; Tian, Y.; Eppler, A. S.; Shen, Y. R.; Somorjai, G. A. *J. Phys. Chem. B* **1999**, *103*, 2935 and references therein.

(8) Kim, D.; Shen, Y. R. *Appl. Phys. Lett.* **1999**, *74*, 3314.

(9) Richter, L. J.; Petralli-Mallow, T. P.; Stephenson, J. C. *Opt. Lett.* **1998**, *23*, 1594.

(10) We identify certain commercial equipment, instruments, or materials in this article to specify adequately the experimental procedure. In no case does such identification imply recommendation or endorsement by the National Institute of Standards and Technology nor does it imply that the materials or equipment identified are necessarily the best available for the purpose.

(11) Dulcey, C. S.; Georger, J. H., Jr.; Chen, M.-S.; McElvany, S. W.; O'Ferrall, C. E.; Benezra, V. I.; Calvert, J. M. *Langmuir* **1996**, *12* 1638.

(12) Shen, Y. R. *Appl. Phys. B* **1999**, *68*, 295 and references therein.

(13) Wei, X.; Hong, S.-C.; Lvovsky, A. I.; Hermann, H.; Shen, Y. R. *J. Phys. Chem. B* **2000**, *104*, 3349.

(14) Sipe, J. E. *J. Opt. Soc. Am.* **1987**, *B4*, 481.

(15) Jones, R. L.; Kumar, S. K.; Ho, D. L.; Briber, R. M.; Russell, T. P. *Nature* **1999**, *400*, 146. Lin, E. K.; Kolb, R.; Satija, S. K.; Wu, W. L. *Macromolecules.* **1999**, *32* 3753. Wallace, W. E.; van Zanten, J. H.; Wu, W. L. *Phys Rev* **1995**, *E52*, R3329. Hu, H.-W.; Granick, S. *Science* **1992**, *258*, 1339.

(16) Following Wignall, G. D.; Ballard, D. G. H.; Schelton, J. *Eur. Polym. J.* **1974**, *10*, 861: R_g (in nm) = 0.028 (molecular mass in g/mol)$^{0.5}$. For 220.5 kg/mol, R_g = 13 nm.

(17) Butcher, P. N.; Cotter, D. *The Elements of Nonlinear Optics*; Cambridge University Press: Cambridge, 1990; Chapter 4.

(18) Hirose, C.; Akamatsu, N.; Domen, K. *J. Chem. Phys.* **1992**, *96*, 997.

(19) Zhang, D.; Dougal, S.; Yeganeh, M. S. *Polym. Prepr.* **1999**, *40***,** 226; *Langmuir* **2000**, *16*, 4528.

(20) Bevington, P. R. *Data Reduction and Error Analysis for the Physical Sciences*; McGraw-Hill: New York, 1969; p 242.

(21) Wilson, E. B. *Phys. Rev.* **1934**, *45*, 706.

(22) Liang, C. Y.; Krimm, S. *J. Polym. Sci.* **1958**, *27*, 241; Sears, W. M.; Hunt, J. L.; Stevens, J. R. *J. Chem. Phys.* **1981**, *75*, 1589.

(23) Both HF and DFT calculations with the B3LYP functional were performed with the 6-311G(2d,2p) basis set with Gaussian 98.

(24) Palafox, M. A. *Int. J. Quantum Chem.* **2000**, *77*, 661.

(25) Goodman, L.; Ozkabak, A. G.; Thakur, S. N. *J. Phys. Chem.* **1991**, *95*, 9044. Ozkabak, A. G.; Thakur, S. N.; Goodman, L. *Int. J. Quantum Chem.* **1991**, *39*, 411. Goodman, L.; Ozkabak, A. G.; Wilberg, K. B. *J. Chem. Phys.* **1989**, *91*, 2069.

(26) Varsanyi, G. *Vibrational Spectra of Benzene Derivatives*; Academic Press: New York, 1969.

(27) Miani, A.; Cané, E.; Palmieri, P.; Trombetti, A.; Handy, N. C. *J. Chem. Phys.* **2000**, *112* 248 and references therein.

(28) Kemnitz, K.; Bhattacharyya, K.; Hicks, J. M.; Pinto, G. R.; Eisenthal, K. B.; Heinz, T. F. *Chem. Phys. Lett.* **1986**, *131*, 285. Ward, R. N.; Davies, P. B.; Bain, C. D. *J. Phys. Chem.* **1993**, *97*, 7141. Gragson, D. E.; Richmond, G. L. *J. Phys. Chem. B* **1998**, *102* 3847.

(29) Durig, J. R.; Hellams, K. L.; Mulligan, J. H. *Spectrochim. Acta* **1972**, *28A*, 1039.

(30) Whiffen, D. H. *Proc. Phys. Soc.* **1956**, *69A*, 375.

(31) Ward, R. N.; Duffy, D. C.; Bell, G. R.; Bain, C. D. *Mol. Phys.* **1996**, *88*, 269.

(32) Simpson, G. J.; Rowlen, K. L. *Acc. Chem. Res.* **2000**, *33*, 781.

(33) Simpson, G. J.; Rowlen, K. L. *J. Am. Chem. Soc.* **1999**, *121*, 2635.

(34) Mansfield, K. F.; Theodorou, D. N. *Macromolecules* **1990**, *23*, 4430.

(35) Ueno, N.; Azuma, Y.; Tsutsi, M.; Okudaira, K.; Harada, Y. *Jpn. J. Appl. Phys.* **1998**, *37*, 4979.

(36) Stöhr, J.; Samat, M. G. *J. Elec. Spectroc. Relat. Phenom.* **1999**, *98*, 189.

(37) Fischer, D. A.; Mitchell, G. E.; Yeh, T. A.; Gland, J. L. *Appl. Surf. Sci.* **1998**, *133*, 58.

(38) Wei, X.; Hong, S.-C.; Zhuang, X.; Goto, T.; Shen, Y. R. *Phys. Rev. E.* **2000**, *62*, 5160.